Title

Prediction of progression in idiopathic pulmonary fibrosis using CT scans atbaseline: A quantum particle swarm optimization - Random forest approach

Authors

Shi, Yu
Wong, Weng Kee
Goldin, Jonathan G.
et al.

Publication Date

2019-08-19

DOI

10.1016/j.artmed.2019.101709

Peer reviewed

Artificial Intelligence In Medicine 100 (2019) 101709

Contents lists available at ScienceDirect

Artificial Intelligence In Medicine

journal homepage: www.elsevier.com/locate/artmed

Prediction of progression in idiopathic pulmonary fibrosis using CT scans at baseline: A quantum particle swarm optimization - Random forest approach

Yu Shi[a], Weng Kee Wong[a], Jonathan G. Goldin[b], Matthew S. Brown[b], Grace Hyun J. Kim[a,b,*]

[a] Department of Biostatistics, University of California Los Angeles, USA
[b] Department of Radiological Sciences, University of California Los Angeles, USA

ARTICLE INFO

Keywords:
Biomedical imaging
Texture features
Wrapper methods

ABSTRACT

Idiopathic pulmonary fibrosis (IPF) is a fatal lung disease characterized by an unpredictable progressive decline in lung function. Natural history of IPF is unknown and the prediction of disease progression at the time of diagnosis is notoriously difficult. High resolution computed tomography (HRCT) has been used for the diagnosis of IPF, but not generally for monitoring purpose. The objective of this work is to develop a novel predictive model for the radiological progression pattern at voxel-wise level using only baseline HRCT scans. Mainly, there are two challenges: (a) obtaining a data set of features for region of interest (ROI) on baseline HRCT scans and their follow-up status; and (b) simultaneously selecting important features from high-dimensional space, and optimizing the prediction performance. We resolved the first challenge by implementing a study design and having an expert radiologist contour ROIs at baseline scans, depending on its progression status in follow-up visits. For the second challenge, we integrated the feature selection with prediction by developing an algorithm using a wrapper method that combines quantum particle swarm optimization to select a small number of features with random forest to classify early patterns of progression. We applied our proposed algorithm to analyze anonymized HRCT images from 50 IPF subjects from a multi-center clinical trial. We showed that it yields a parsimonious model with 81.8% sensitivity, 82.2% specificity and an overall accuracy rate of 82.1% at the ROI level. These results are superior to other popular feature selections and classification methods, in that our method produces higher accuracy in prediction of progression and more balanced sensitivity and specificity with a smaller number of selected features. Our work is the first approach to show that it is possible to use only baseline HRCT scans to predict progressive ROIs at 6 months to 1year follow-ups using artificial intelligence.

1. Introduction

Idiopathic Pulmonary Fibrosis (IPF) is a chronic irreversible and ultimately fatal disease of unknown etiology. It is characterized by an unpredictable progressive decline in lung function and typically affects people in the age group of 50–70 years. From 2001–2011, among newly diagnosed IPF subjects with Medicare, the median survival time was 3.8 years [1]. Potential risk factors include smoking, environmental exposures, and microbial agents [2]. The disease is characterized by respiratory symptoms such as shortness of breath, a dry cough, and fatigue, reduced pulmonary function test results, and fibrosis patterns on HRCT [2]. The disease exhibits a highly heterogeneous natural history, and the disease progression is unpredictable at the time of diagnosis: some subjects may experience episodes of acute respiratory worsening despite being previously stable [2]. It is critically important to distinguish subgroups of IPF subjects who are expected to progress from those who are expected to remain stable. The identification helps clinicians to make a decision of continuing or switching a treatment, or to refer for a lung transplantation at an early stage.

High-resolution Computed Tomography (HRCT) plays an important role in the diagnosis of IPF [2]. Studies have shown that HRCT features are useful and sensitive in predicting progression in IPF subjects based on the patterns of usual interstitial pneumonia (UIP) between two scans [3,4]. Research shows that UIP patterns on HRCT are associated with high mortality and disease progression in subjects with IPF [4]. Because of the heterogeneous natural history of IPF, a multidisciplinary team of pulmonologists, radiologists, and pathologists has devoted to build a guidance of diagnostic models of IPF for subjects with interstitial lung

* Corresponding author at: Department of Biostatistics & Radiological Science, University of California Los Angeles, USA.
E-mail address: gracekim@mednet.ucla.edu (G.H.J. Kim).

https://doi.org/10.1016/j.artmed.2019.101709
Received 28 November 2018; Received in revised form 10 August 2019; Accepted 19 August 2019

disease [2]. According to the guidelines, a HRCT scan is required for diagnosis of IPF. Quantitative image analyses (QIA) using texture-based features from HRCT scans have been utilized intensively in pulmonary related diseases [5–7]. For example, QIA are used for robust classification of interstitial lung disease patterns. Scores from QIA can be a good representation of extent of IPF [8]. The models that leverage HRCT quantitative imaging data usually require measurement of changes from baseline to follow up [3]. However, not many subjects from clinical visits have routine HRCT follow-up unless they have experienced shortness of breath or suspicion of progression. Given that HRCT scans are not utilized for monitoring purposes but for confirmation of progression, and subjects with IPF have short median survivals, it would be desirable to develop a prediction model for the IPF progression using only baseline HRCT scans. Features extracted from HRCT images are usually high-dimensional, which pose a challenge for image recognition systems because redundant or non-informative features sometimes reduce classification accuracy. For this reason we need a feature selection procedure to select a subset of important HRCT features to stratify the groups of subjects who are likely to progress or not.

Several methods have been proposed to select features and build classification models in the medical imaging field. Regularization methods, such as least absolute shrinkage and selection operator (LASSO) [9] and smoothly clipped absolute deviation (SCAD) [10], are handy and popular methods in the field [11,12]. The field has seen increasing uses of more advanced techniques [13], such as random forest [14], support vector machine (SVM) [15–17], neural network (NNET) [18], etc. However, most work either has no feature selection step, or separate the feature selection and classification steps, which fail to select the optimized feature subset that leads to the best classification performance.

An appropriate approach to integrate feature selection and classification is a wrapper method, which directly uses the classification performance of a given model to assess selected subsets of features [19]. Efficient search strategies are critical for a wrapper method to identify the best feature subset. Evolutionary computation (EC) has received much attention from the feature selection community because of the good global optimization properties of many state-of-the-art EC-based feature selection techniques. Compared with traditional searching methods, EC techniques do not need domain knowledge and do not make any assumptions about the feature space, such as linear separability and differentiability [19]. EC is particularly useful in our case because the objective function in our problem does not have an analytical form, and the common optimization techniques which require leveraging mathematical properties of the objective function cannot be used. In this work, we propose to use a type of EC algorithm called quantum-inspired particle swarm optimization (QPSO), coupled with a random forest algorithm (RF) as a wrapper method to build a prediction model that has high accuracy and a good balance between sensitivity and specificity. Inspired by wave functions in quantum physics, QPSO has enhanced searching ability and improved optimization results over many other commonly used EC algorithms [20–24]; empirically, it is superior based on comparative experiments using benchmark test functions [25]. It has been applied in the imaging field in recent years [22,26] and shows promising potential in dealing with high-dimensional imaging data.

To our best knowledge, this work is the first ROI-based computer-aided-diagnostic (CAD) model that can be applied to a baseline HRCT scan for predicting progression at 6 months to 1 year follow-up. Further, the methodological contributions of this work include two aspects: (a) a study design of collecting a data set with ground truth for prediction via visual registration by a radiologist; and (b) the development of an objective metric and an algorithm that simultaneously achieves high prediction accuracy, balanced sensitivity and specificity with a parsimonious feature subset, using a relatively small number of subjects.

2. Background

2.1. Texture features

Texture features extracted from images can be considered as a mathematical characterization of images. They reflect granular spatial information quantitatively. They describe the grey levels of voxels along different orientations as well as spatial relationships of voxels within a local neighborhood. We extract features using a grid sampling procedure described in [7]. Grids composed of 4-by-4 voxel squares were placed contiguously. From each grid, a voxel was selected. The grid sampling was used to assure complete coverage of regions of interest. We extract 71 imaging features from each sampled voxel (See the Appendix 1 for details in computations).

While deep learning has gained popularity in the medical imaging field recently, it suffers from overfitting and underfitting problems when the training samples are small [27]. Deep learning framework is not practical to our design of data collection, because of costly and laborious ROI markings from radiologists' visual assessments even for a small sample size. Alternatively, a promising approach is a wrapper method with a machine learning algorithm in the task of texture feature selection and classification. In the following sections, we show that this approach is feasible and can provide markedly improved results, relative to currently available methods.

2.2. Feature selection

In classification problems, a critical step is to carefully select a small number of features for prediction. This selected subset of features can substantially reduce the processing time, and give robust and superior results to using the full set of features [28]. Selecting a subset that gives the best performance in classification is challenging. In our problem, there are 2^{71} possible subsets and an exhaustive search for the best subset is impossible. Further complicating matters, there are complex interactions among the features. Fig. 1 shows the 71 texture features on the horizontal and vertical axes. The color shades show the magnitude of their paired Pearson correlations. There is no clear pattern of the correlations and it is hard to screen and eliminate highly correlated predictors. Traditional methods that assume a linear relationship between the outcome and a set of additive variables may not be applicable to our data set.

In feature selection, there are broadly two types of algorithms: filter

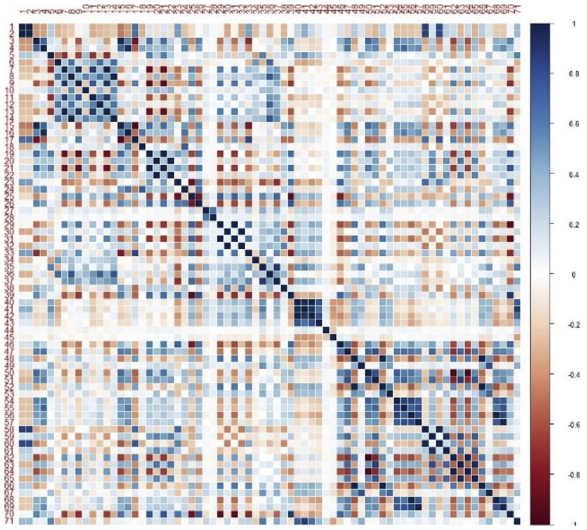

Fig. 1. Horizontal and vertical axes show 71 texture features. Pearson correlation coefficients were calculated for each pair and the color shades show the magnitude of the correlations.

methods and wrapper methods. Filter methods assess the relevance of features by looking only at the intrinsic properties of the data [29,30]. For example, stepwise regression adds or eliminates individual variables sequentially until there is no statistically significant change in model performance. The selected variables then serve as inputs to the classification algorithm. Filter methods separate feature selection from classification, and typically, feature selection is performed only once before the classification task. The main advantage of filter techniques is that they are computationally simple and fast. However, filter methods ignore the interactions of the feature selection step with the classification step, which may result in a compromised classification performance [31].

Different from filter methods, wrapper methods evaluate predictors holistically using procedures that add and/or remove predictors simultaneously, in order to find a combination that optimizes the performance [32,33]. Wrapper methods treat different feature subsets as inputs and the performance of the models as outputs [34,35]. There are two components in a wrapper method: an optimizer and a classifier. The metrics from the classifier serve as the objective function for the optimizer to search the best feature subset. Compared to filter methods, wrapper methods are usually computationally expensive because many candidates of subsets have to be evaluated against the previous best subset [36]. Wrapper methods also have a higher risk of overfitting due to the lack of established criteria of a penalized function [31]. On the other hand, wrapper methods are able to directly relate feature subsets to the classification performance. They include the interaction between feature subset search and model selection, and they are able to take into account feature dependencies [31].

2.3. QPSO as an optimizer in wrapper method

Evolutionary Computation (EC) has been shown to be useful as an optimizer in wrapper methods to search the feature space and find feature subsets that optimize the classification performance. See [19] for a comprehensive summary and comparison of EC applications in feature selection. Particle swarm optimization (PSO) is a widely used EC algorithm that does not impose any assumption on the objective functions. Proposed in 1995 [37], PSO was inspired by swarm intelligence: a swarm collectively acts and communicates so that a good solution can be found quickly. There are many variants of PSO, and quantum PSO is one of them [20]. Inspired by basic particle movements in the quantum mechanics framework, QPSO is a global optimization algorithm with superior searching capabilities compared to other EC algorithms [21]. It is different from traditional PSO algorithms in that particles have no trajectory, instead, the particles appear in positions with probabilities. See [21] for a comprehensive summary of the characteristics and properties of the QPSO algorithm. The QPSO algorithm is suitable in our situation due to its superior capability in searching high-dimensional space and its successful applications in real-world problems including those in the imaging field [22,26].

To prevent QPSO from premature convergence, we also enhanced the algorithm by using probabilistic cross-over operations and random mutation operations, as cross-over and mutation operators have shown to improve the PSO performance in feature selection [38]. We coded each particle in QPSO using a binary coding scheme. As an example, suppose a feature space has 5 features and a particle is encoded as (1, 0, 0, 1, 1). This means that the 1st, 4th, and 5th features are included and the 2nd and 3rd are excluded in selection.

3. Material and methods

In the objective of this work, we want to build a prediction model that has a good balance between sensitivity and specificity. The previous IPF studies in machine learning have often focused on improving sensitivities, as it is clinically meaningful to detect progression, when there were no effective therapeutic treatments [39,40]. With effective anti-fibrotic IPF therapeutic treatments now being available [41], there is an increasing need to understand the early signs of improvement or stabilization (not only progression), which led to the need of optimizing specificity. As such, we developed an objective metric to be maximized as the minimum

of sensitivity and specificity. This metric is beneficial for a balanced classification. We compare the proposed algorithm to other wrappers and non-wrapper methods in terms of accuracy, sensitivity, specificity, and number of selected features.

3.1. Dataset acquisition

A total of 50 anonymized HRCT images of subjects with IPF from a multi-center clinical trial were selected and at least two scans were available for each subject for the model building purpose. We collected a data set with well-characterized HRCT scans from subjects of IPF and the dates of baseline scan ranged from 2011 to 2015. Anonymized HRCT images of these subjects were archived at the UCLA Computer Vision and Imaging Biomarkers Laboratory. The use of anonymous image data was approved by local institutional review board. The population had a mean age of 65.9 years and a mean forced vital capacity (FVC) percentage predicted value of 69.2%.

We collected a baseline scan and a 7.3 month (SE ± 1.6 months) follow-up HRCT scan from each subject with IPF. The first task is for a radiologist to visually mark ground truth of the regions of interest (ROI) at baseline scans in order to collect the textural information. Three steps of radiologist's assessment were: (1) a thoracic radiologist (JGG, 20+ years of experience with expertise in diffuse lung disease) identified the ROI in chest CT as reflecting progression or non-progression by reviewing the two paired longitudinal HRCT scans; (2) contoured the ROI at *baseline* scan (before the changes occurred), the ROIs were contoured to avoid airways and blood vessels; and (3) labeled the ROI type as progression or non-progression. The visual registration matches the baseline and follow-up in the anatomical correspondence of ROIs. This step was performed by the radiologist.

Table 1 provides the baseline characteristics of the subject population by ROI status, namely, whether or not subjects had at least one progressed ROI. Demographic profiles and the percent predicted FVC between the two groups are comparable. Quantitative lung fibrosis (QLF) is a classifier-model-derived score and is a measure of baseline disease extent [8]. The means of QLF scores were also similar between two groups who had progressed ROI and those who had no progressed ROI. This suggests that the progression at the ROI level provides insights beyond disease extent and visual patterns of IPF, and is promising for detecting early signs of disease progression. Within each contoured ROI, a square of 4-by-4 grid sampling was implemented to generate voxel instances, and texture features were calculated based on these

Table 1
Baseline characteristics of the subject population.

	Visual assessment	
	Subject with ≥1 progressed ROI	Subject with no progressed ROI
# Subjects	33	17
# ROIs	166	84
# Progression ROIs	72	0
# Non-progression ROIs	94	84
Age (mean ± SE), years	66.7 ± 7.7	68.1 ± 7.1
% of Female	17	23
Baseline % predicted FVC (mean ± SE), %	68.7 ± 3.3	69.8 ± 2.8
Follow up % predicted FVC (mean ± SE), %	63.2 ± 3.0	67.8 ± 2.4
Baseline QLF (mean ± SE), %	14.2 ± 1.4	13.4 ± 1.4
Follow up QLF (mean ± SE), %	16.1 ± 1.8	15.3 ± 1.7

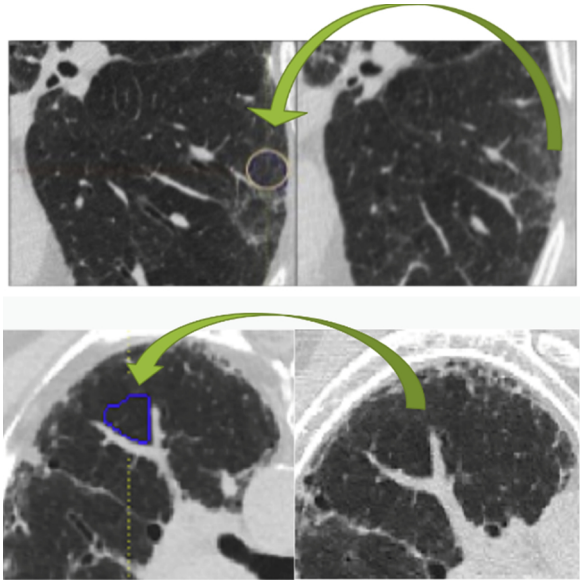

Fig. 2. a (top). The baseline and follow-up HRCT of an IPF subject (progression): a radiologist compared a pair of set of HRCT and chose a classic representative small region and labelled the progression status based on the changes in imaging patterns. The contoured area in the HRCT scan at baseline is an example of region as *expected to be progressed*. Fig. 2b (bottom). The baseline and follow-up HRCT scans of an IPF subject (non-progression): similarly, a radiologist compared the baseline ROI and its anatomical match in the follow-up scan and determined the pattern as non-progression. The contoured area at baseline is contoured as an *expected to be stable (not-progressed)*.

local neighborhoods of voxels. See [7,42–44] for texture feature computation details.

Importantly, the radiologist labeled a ROI on the *baseline* scan (before the changes occurred) as "expected to be progressed" if the ROI got worse in the follow-up scan, or "expected to be non-progression" if the ROI got better or stayed stable on the follow-up scan. Fig. 2 depicts this data procedure of acquisition where Fig. 2a and b indicate the expected progressive and non-progressive ROIs in the follow-ups, respectively. We say that our model is *predictive* because texture features were only obtained from baseline scans when we built the classification model. The model is evaluated and compared with the ground truth obtained by a thoracic radiologist assessment. The procedure of data acquisition enables a supervised learning approach since we collected HRCT images from subjects with follow-up scans. The ultimate application of this algorithm is to predict a subject's status for those who does not necessarily have follow-up scans.

3.2. Feature selection and classification methodology

3.2.1. The objective function

Empirically, directly optimizing accuracy of classification would produce a skewed result with high specificity and low sensitivity, since non-progression is the majority class and specificity is the main driver of accuracy in an unbalanced data. To build a more balanced classifier, we need to consider a composite metric that includes both sensitivity and specificity. In computer science, a commonly used metric is F_1 score, which is a harmonic mean of precision and recall. One can think of F_1 score as a smoothed minimum of precision and recall [45]. However, F_1 score only compromises mildly when we have unbalanced classification results.

In this work, we propose a new objective metric to maximize the minimum of the sensitivity and specificity, produced by the classification algorithm. To our best knowledge, there is only one similar metric in the 2012 PhysioNet/Computing in Cardiology Challenge [46], which sought to maximize the minimum of positive predictive value (also known as precision) and sensitivity (also known as recall). Their choice stimulated competitors to optimize the Precision-Recall (PR) curve of classifiers, whereas our metric optimize the usual receiver operating curve (ROC). The classification results on our data set suggest that this metric is beneficial for a balanced sensitivity and specificity. Specifically, the objective is

$$\underset{F_s}{argmaxmin}(sensitivity, specificity)$$

Where $\boldsymbol{F_s}$ is any feature subset, and both sensitivity and specificity are classification metrics on the test set returned by the classification algorithm built upon $\boldsymbol{F_s}$.

The solution to this optimization problem does not have an analytical form, which means that it is hard to derive mathematical properties, such as convexity or differentiability of the objective function. Consequently, we resort to heuristic algorithms such as QPSO, and show that it can be particularly useful in this case.

3.2.2. The optimizer

To gain superior performance in prediction, we use the QPSO algorithm (see Algorithm 1 in Appendix 2). In theory, the algorithm converges to the global optimum when parameters are appropriately chosen and the number of iterations approaches infinity [21]. Steps of QPSO and algorithm convergence proof are available in [47].

The parameters in our QPSO algorithm are the same as those recommended in [48]: the number of particles is 40, the dimension of each particle is 71 (as we have 71 features), the maximum number of iterations is 1000 and each iteration involves 5-dimensional mutation at any one time (See the steps 1–5 in Algorithm 1). The choices of the number of particles and the maximum number of iterations follow the convention, which were used and suggested in many PSO literatures for their good performance on the benchmark functions [49,50]. A binary encoded

QPSO determines the probability of flips using a function in step 6 in Algorithm 1, which is inspired by a wave function in quantum mechanics [20]. We note that the solution may not be optimal or unique, as in practice we use only a limited number of iterations, and there might be several feature subsets that produce the same or similar fitness values, which is a typical problem in feature selection.

3.2.3. The classifier

We build the classification model based on selected features using the random forest algorithm [51]. Research has shown that tree-ensemble-based machine learning techniques such as random forest are effective for solving real world problems [52–54]. Random forest has also been widely used in the medical imaging field and is highly successful in many classification tasks [14,55]. For high-dimensional data, random forest is easily applicable in distributed systems. A random forest classifier is particularly suitable for our problem because: 1) it is computationally fast and reasonably easy to train for high-dimensional data; 2) it minimizes storage, and this is especially important in our future work when we want to scale our algorithm to expand to whole lung level as is discussed in section 5; and 3) it tends to provide feature diversity, which is particularly important when dealing with heterogeneous data [56].

The parameters we used in the random forest classifier were set as follows: the maximum depth of each tree is 20, the number of trees is 100, the proportions of subsample from the data set is 0.5, and the proportion of features randomly selected at each node of each tree is 0.5. The guidelines for selecting parameters such as tree depth, forest size and sampling density remain an open question [14]. Since we have 71 features in total, a depth of 20 uses up to 30% features in individual trees and seems to be sufficient in our case. We also observe that when the depth further grows, RF tends to overfit, compromising the classification results. The choice of the number of trees considered the

computational budget of running the experiments.

3.2.4. The resampler

We observe pattern imbalance in our data set, which is a common problem in machine learning. Imbalance in classes can have significant impact on performance, especially for minority classes. Re-sampling is a routinely used pre-processing technique in statistics [57] to enhance frequencies in minority classes to obtain a balanced performance in classification. Various re-sampling techniques have been developed in biomedical imaging studies. Two general re-sampling approaches are up-sampling and down-sampling. Up-sampling is any technique that simulates or imputes additional data points, and down-sampling refers to any technique that reduces the number of samples to improve the balance across classes. Research has shown that a combination of over-sampling the minority class and under-sampling the majority class, such as a synthetic minority over-sampling technique (SMOTE) [58], can achieve better classification performance than using either alone. In SMOTE, the over-sampling is to sample "synthetic" examples with inversely proportional weights of sample size in order to balance the ratio of classes, rather than sampling with replacement. The majority class is under-sampled by randomly removing samples from the population until the minority class becomes some user-specified percentage of the majority class. In this work, we apply SMOTE on the training set only and independently apply the classifier to the test set to be consistent with the nature of the data. The resampled training data set has perfectly balanced frequencies for progression and non-progression voxels.

3.2.5. Quantum PSO - random forest (QPSO-RF) algorithm

In this section, we propose QPSO-RF as an integrated wrapper algorithm that performs HRCT texture feature selection and imaging pattern prediction effectively. Steps of the proposed algorithm are shown in Algorithm 1. First in the *resampling* step, we use SMOTE to resample the training set. We then use QPSO as the optimizer to search the feature subsets (Step: 1–6), and random forests are built upon 40 selected subsets (Step: 7–12) which produces the evaluation metrics. The iterative process of QPSO-RF searches the feature space in all the particle best (*pbest*) and returns the global best (*gbest*) at the last iteration as the best feature subset that gives the maximized objective function.

Fig. 3 shows the flowchart of the QPSO-RF algorithm, which describes the steps of the algorithm. QPSO-RF uses the QPSO to select features from a resampled data set to build a random forest classifier, and uses the objective function to guide the algorithm to find a best feature subset.

3.2.6. Statistical analysis of the results

We implemented statistical procedures to test if the differences of prediction accuracy between the proposed QPSO-RF and other comparator methods were statistically significant. We used conditional logistic regression models for analysis, which is a standard method for analyzing matched case-control data [59]. The outcome is whether the ROI prediction is accurate (binary), and the covariate is the indicator of method. Since each subject may contribute multiple ROIs, we used a clustered sandwich estimator as the variance structure. The clustered sandwich estimator allows for intragroup correlation within ROIs that were from the same subjects, and maintains the independence across ROIs from different subjects [60]. The p-values for each model's coefficient are reported in Tables 2 and 3.

We also addressed the multiple comparison using a Benjamini–Hochberg procedure controlling the false discover rate (FDR) at 0.05 significance level [61]. In total, we have 23 pairwise comparisons of the proposed algorithm to comparators trained on re-sampled or original training data set.

4. Results

We split the data into a training set and a test set. The training set had 26 subjects, and the test set had a different group of 24 subjects. The training set had 77 non-progression and 50 progression ROIs, adding up to 127 ROIs; at the voxel level the training set had 1172 non-progression and 582 progression voxels, adding up to 1754 voxels. The test set had 101 non-progression and 22 progression ROIs, adding up to 123 ROIs; at the voxel level the test set had 1605 non-progression and 336 progression voxels, adding up to 1941 voxels. In our data set, the progression and non-progression lung morphology outcomes had an unbalanced ratio. At the voxel level the ratio was 1:3 (918 progression: 2777 non-progression instances) and at the ROI level the ratio was 1:2.5 (72 progression vs 178 non-progression). For the training set we applied the re-sampling SMOTE technique as a class imbalance remedy; the post-SMOTE training set had 1746 progression and 1746 non-progression voxel instances and the model was trained on this re-sampled set. The test set was evaluated without any resampling modifications. Texture features were calculated at the voxel level and the radiologist references were ROI-based; we therefore performed a majority voting strategy to transform the classifier outcome from voxel to ROI level.

4.1. Choices of comparator algorithms

We compared the performance of our algorithm with other feature selection and classification techniques. Firstly we considered a range of wrapper methods that use different optimizers and classifiers. The classifiers used included support vector machine (SVM) and shallow neural network (NNET); classifiers using all features (without feature selection) were also included in the comparison. The optimizers used for comparison included the basic version PSO and the Genetic Algorithm (GA). GA was inspired by the principles of genetics and evolution, and mimics the reproduction behavior observed in biological populations [62]. The GA employs the "survival of the fittest" principle in its search process to select and generate individuals (in our case, feature subsets) that are adapted to their environment (objectives). The desirable traits tend to over-express over a number of generations (iterations), leading to better and better solutions. GA has also been frequently used in feature selection problems [63]. Research has shown that PSO has the same effectiveness as a Genetic Algorithm (GA) with significantly improved computational efficiency [64].

We also compared the method to non-wrapper, model-based methods including LASSO and SCAD. LASSO and SCAD were used to perform feature selection by employing penalties. They have been widely adopted and can effectively enhance the prediction performance of the regression model [11,12].

The comparators used in this work are commonly used methods in the medical imaging field [13] and have comparable computational efforts. The configurations of each comparator algorithm were set as follows. For LASSO and SCAD, we standardized the feature set and then used cross validation to choose the best penalty parameters for prediction. We then applied the cross-validated LASSO or SCAD model to the test set. For GA, we used 1000 iterations, 40 populations, cross over rate of 0.8 and mutation rate of 0.02, which was comparable to QPSO and PSO parameter settings. For SVM, we used a Gaussian radial basis function (RBF) kernel with a scaling factor 1 [16,17]. For NNET, we used a two-layer feedforward network with 10 hidden-layer neurons, a sigmoid transfer function in the hidden layer, and a softmax transfer function in the output layer [18]. These parameters for the comparator optimizers and classifiers were pre-specified based on the computational feasibility consideration as well as best practices reported in literature.

Despite our best intent to compare the proposed methods to other methods used in feature selection and classification tasks, it was hard to do an exhaustive comparison. Potentially, there could be other methods that are even more effective in our data set.

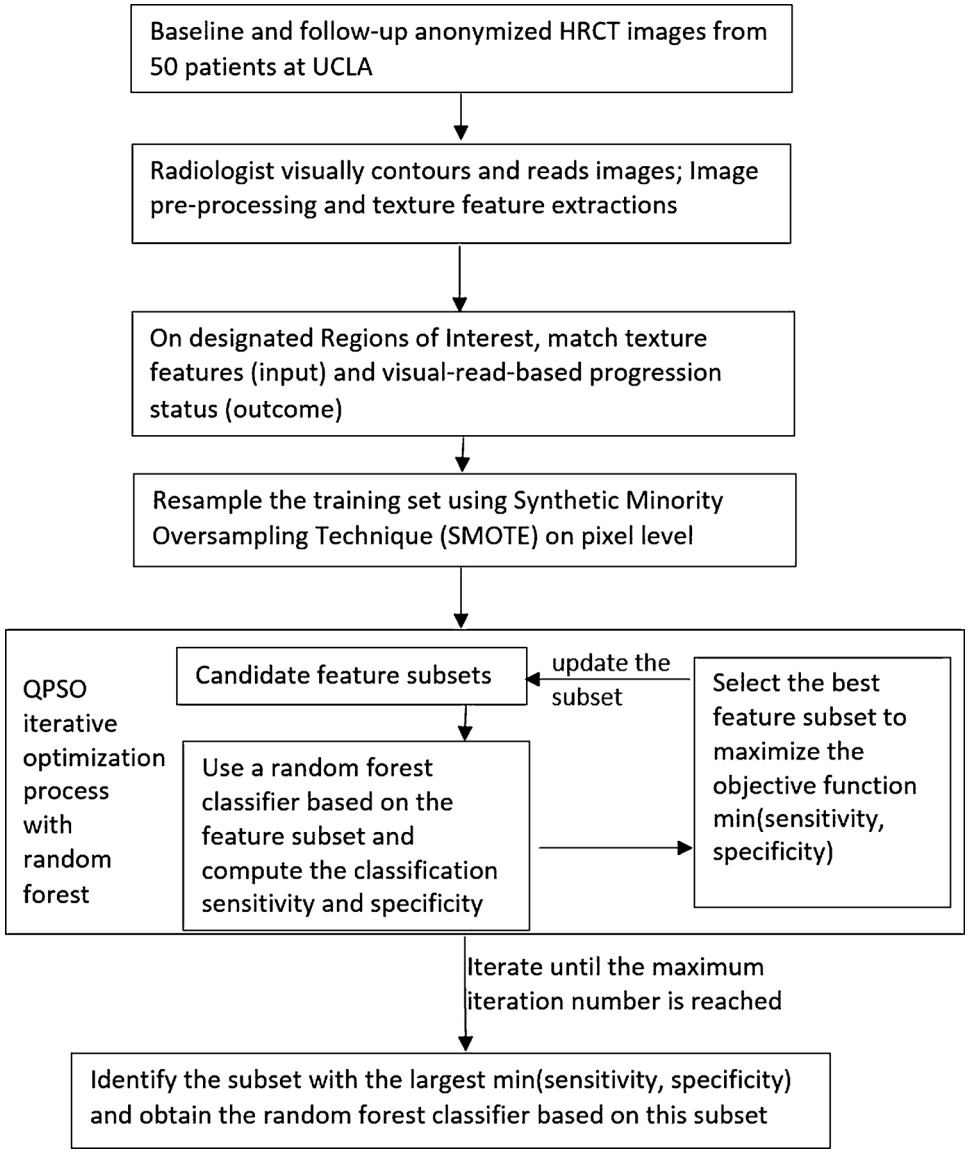

Fig. 3. Flowchart of random forest QPSO-RF algorithm for IPF prediction.

Table 2
Classification results from different algorithms applied on the test set using SMOTE in the training set. Wrapper methods are displayed in optimizer-classifier format. P-value comparing each method to QPSO-RF is based on conditional logistic regressions. Asterisk indicates significance after controlling the overall false discovery rate at 0.05 significance level. $p < 0.05$: * (significant); $p < 0.01$: ** (very significant); $p < 0.001$: *** (highly significant).

	Sensitivity	Specificity	Accuracy	P-value		# features
QPSO-RF	0.818	0.822	0.821			19
LASSO	0.864	0.554	0.610	< 0.001	***	56
SCAD	0.818	0.564	0.610	< 0.001	***	47
RF w/o feature selection	0.727	0.723	0.724	0.022	*	71
SVM w/o feature selection	0.000	1.000	0.820	1.000		71
NNET w/o feature selection	0.727	0.574	0.602	0.001	**	71
PSO-RF	0.864	0.663	0.699	0.004	**	29
PSO-SVM	0.864	0.653	0.691	0.017	*	39
PSO-NNET	0.818	0.594	0.634	0.001	**	39
GA-RF	0.909	0.584	0.642	0.001	**	38
GA-SVM	0.864	0.663	0.699	0.019	*	36
GA-NNET	0.909	0.604	0.659	0.001	**	37

Table 3
Classification results from different algorithms applied on the test set without SMOTE in the training set. Wrapper methods are displayed in optimizer-classifier format. P-value comparing each method to resampled QPSO-RF is based on conditional logistic regressions. Asterisk indicates significance after controlling the overall false discovery rate at the 0.05 significance level. $p < 0.05$: * (significant); $p < 0.01$: ** (very significant); $p < 0.001$: *** (highly significant).

	Sensitivity	Specificity	Accuracy	P-value		# Features
QPSO-RF	0.727	0.762	0.756	0.159		30
LASSO	0.636	0.713	0.711	0.024	*	54
SCAD	0.682	0.772	0.756	0.108		10
RF w/o feature selection	0.682	0.802	0.780	0.367		71
SVM w/o feature selection	0.909	0.644	0.691	0.012	*	71
NNET w/o feature selection	0.727	0.733	0.732	0.016	*	71
PSO-RF	0.818	0.743	0.756	0.089		48
PSO-SVM	0.909	0.644	0.691	0.017	*	20
PSO-NNET	0.682	0.792	0.772	0.241		39
GA-RF	0.682	0.762	0.748	0.097		38
GA-SVM	0.864	0.693	0.724	0.032	*	31
GA-NNET	0.636	0.733	0.727	0.012	*	29

4.2. Comparisons of classification performances

The QPSO-RF algorithm yielded a model with 19 texture features and achieved 81.8% sensitivity, 82.2% specificity and 82.1% accuracy at the ROI level on the test set in predicting progression at 6 months to 1 year follow-ups. Table 2 compares the results from different methods trained on resampled training sets and then applied on the test set. It is clear that QPSO-RF is superior compared to other wrapper methods and model-based methods, in a sense that QPSO-RF selects a smaller set of texture features than most of the other algorithms, has a higher and more balanced classification sensitivity and specificity, and has higher accuracy. Compared to LASSO, SCAD, other wrapper methods, and classification models without feature selection, QPSO-RF provides the only solution that both sensitivity and specificity achieves above 80%. It also achieves the highest classification accuracy with the smallest feature set. Using conditional logistic regressions and controlling the overall FDR at the significance 5% level, we see that QPSO-RF accuracy is statistically significantly higher than all other methods except for the SVM without feature selection; the latter method is not ideal because it classifies all ROIs as non-progression. The QPSO-RF selected features include 2 summary statistical features, mean and mean32 (gray-level mean of 32 brightest voxels), and 17 Gy-level co-occurrence matrices (GLCM) features. These features are important to understand the characteristics of the images and are good representations of the images.

In addition, a re-sampling technique is helpful to achieve better classification results. Table 3 compares results from same comparators trained without resampling. There is no method that achieves above 80% for both sensitivity and specificity. The resampled QPSO-RF achieves statistically significantly higher classification accuracy than six other methods in Table 3. Generally, wrappers trained without re-sampling produce higher specificity, but much lower sensitivity and reduced overall accuracy compared with the wrappers trained with resampling. This is because that the data without resampling has under-representative progression class, and as a result, it's hard for the models to pick up the minority class. In particular, if QPSO-RF was applied without re-sampling, 30 features were selected and the sensitivity dropped to 72.7%, specificity dropped to 76.2%, with overall accuracy reduced to 75.6%. We note that compared to other algorithms in Table 3, QPSO-RF without SMOTE still achieves one of the highest accuracy levels, balanced sensitivity and specificity, and select one of the smallest feature sets.

Empirically, random forest was to be the superior classifier in our data set. On the resampled data set, RF (without feature selection) and PSO-RF had the highest accuracy among all methods following QPSO-RF; on the data set without resampling, RF (without feature selection) had the highest classification accuracy, and QPSO-RF and PSO-RF also had higher accuracy than most other methods. These results suggest that RF is a superior classifier for this data set. Further, QPSO method was found to be the best optimizer for our data set, and it selected a parsimonious feature subset compared to PSO and GA optimizers. As a result, the resampled QPSO-RF was found to be clearly a superior method that achieved all of our goals of high accuracy, balanced sensitivity and specificity, with a smaller number of selected features.

Fig. 4 provides a visual representation of our classification procedure of 6 ROI sample cases. We constructed this figure based on the coordinates of each voxel, which then enabled us to visualize the voxel level classification within each ROI. Our algorithm correctly classified ROI patterns in case 1–4 cases but misclassified in case 5 and 6. Case 1 is a non-progression ROI, and QPSO-RF correctly classified 97.4% voxels as non-progression, which transformed to a "non-progression" label correctly to the ROI. Case 2 is a progression ROI with 83.3% voxels classified correctly as progression to the ROI. Case 3 is another non-progression ROI, with 83.3% voxels classified as non-progression and the case is correctly classified. Case 4 is a progression ROI and 86.7% voxels are classified correctly and the case is correctly classified as a progression ROI. Case 5 is a progression ROI with 62.5% voxels classified as non-progression, which transformed to a "non-progression" label to the ROI. Case 6 is a non-progression ROI with 85.7% voxels misclassified as progression ROI.

In summary, our proposed algorithm works well for our data set in that it outperforms other methods by giving higher accuracy, higher and more balanced sensitivity and specificity, with a smaller number of selected features. The ROI-based prediction provides insights beyond disease extent and visual parenchymal patterns of IPF.

5. Discussion

We show that a QPSO-RF algorithm can predict the IPF progression using baseline HRCT scans, where QPSO-RF algorithm integrated feature selection and pattern recognition. The proposed QPSO-RF algorithm had superior prediction performances on our data set, compared to commonly used methods in machine learning [13–17]. The QPSO-RF methodology with the appropriate study design of reference data collection makes it possible to predict IPF disease progression at 6 months to 1 year follow-up on HRCT scans using a baseline HRCT. For subjects with IPF, accurate prediction of disease progression is crucial for the appropriate medical intervention at time of diagnosis. Similar data sets for IPF subjects are rarely available, pending for external validation of the algorithm with other independent data sets. We expect our algorithm will also perform well for other data sets based on representative data and parsimonious methods.

We expect that the performance of this algorithm can improve further with additional information of age, gender, and the pulmonary function tests (PFT), which have been shown to be useful for IPF prognostication [65]. Adding the information in a short time period with baseline HRCT scan, prediction results may improve in long-term follow-ups.

In Fig. 4, the misclassified cases might be attributed to faster than usual progression (case 5), and the clinical fact that honeycomb rarely progresses to the next level (case 6). Further, we observe that the classification relies on the number of voxels within each ROI and this may affect the classification of ROI-level. This means that the error tolerance is low for ROIs with a few voxels. One potential way to tackle this issue is to expand this algorithm from the voxel level to the whole lung scan to achieve more robust classification.

Fig. 5 is an example of the expansion of the current algorithm. The

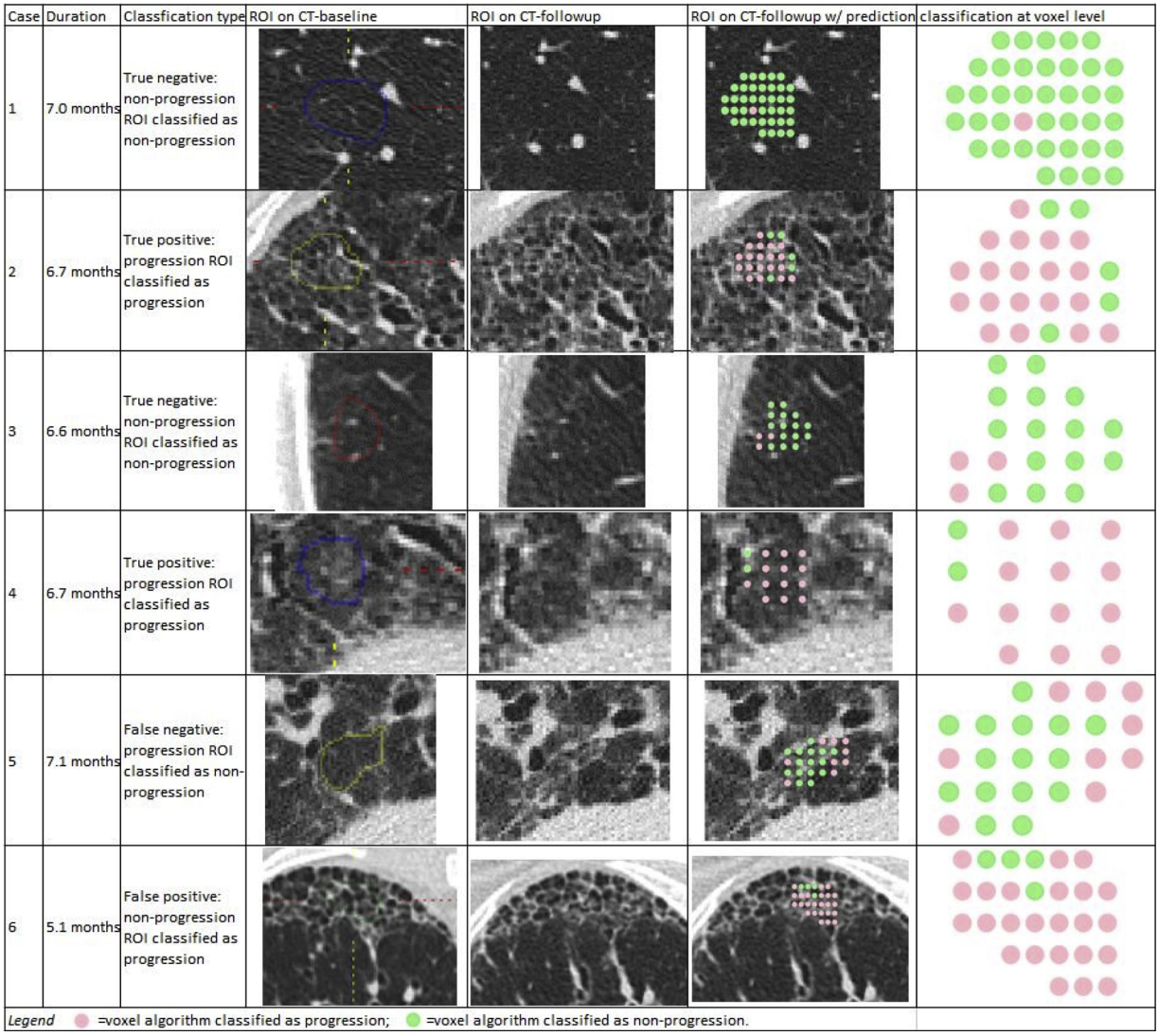

Fig. 4. Classification results visualization: dots with (green) light intensity = voxels QPSO-RF classified as non-progression, dots with (red) dark intensity = voxels QPSO-RF classified as progression. Case 1–4 are correctly classified cases, case 5 and 6 are misclassified cases.

subject experienced extensive disease progression in the 9 month follow-up period with 8.4% increase in QLF and 7% decrease in the percent of predicted FVC, and the expanded prediction algorithm successfully picked up 75.4% of progression voxels based on the baseline scan. The prediction in whole lung eliminates the bias of ROI contouring and makes the prediction robust. The expansion could be automated in the prediction process with little radiologist input. Research has shown that quantitative scores that are summated for the whole lung correlates with PFT results, and is related to extent and severity of interstitial lung disease [66]. Current work shows some promising results, yet the clinical validation is under development.

There are several limitations of the study. Firstly, we have a relatively small sample size. This is part of an initial study for testing feasibility. Secondly, the performance of the model is limited to the classical representation of small ROIs. Thirdly, the reference of gold standard was based on a single reader's visual assessment. Analytical and clinical validations are warranted in future to evaluate a predictive biomarker and to test the generalizability of algorithm to the whole lung. Further, we only compared our algorithm to selected popular methods, with parameters reported as best practices in literature. There are possibly better implementations of comparator methods, or other methods that are also suitable for our problem. Lastly, we did not perform cross-validation within the training set.

6. Conclusion

We developed a new approach to predict disease progression on HRCT images using only metrics at single scan for subjects with IPF. Our study design for data acquisition provided the first data set of IPF prediction using baseline HRCT scans at ROI level. We also developed an integrated algorithm of texture feature selection and pattern prediction, which yielded superior results, in terms of high accuracy, balanced sensitivity and specificity, with a small feature subset for predicting parenchymal progression.

Declaration of Competing Interest

None.

Acknowledgments

This work was partially supported by the National Heart, Lung, and Blood Institute of the National Institutes of Health under the Award Number R21HL123477-01A1, and by the National Institute of General Medical Sciences under the Award Number R01GM107639. The content is solely the responsibility of the authors and does not necessarily represent the official views of the National Institutes of Health. The

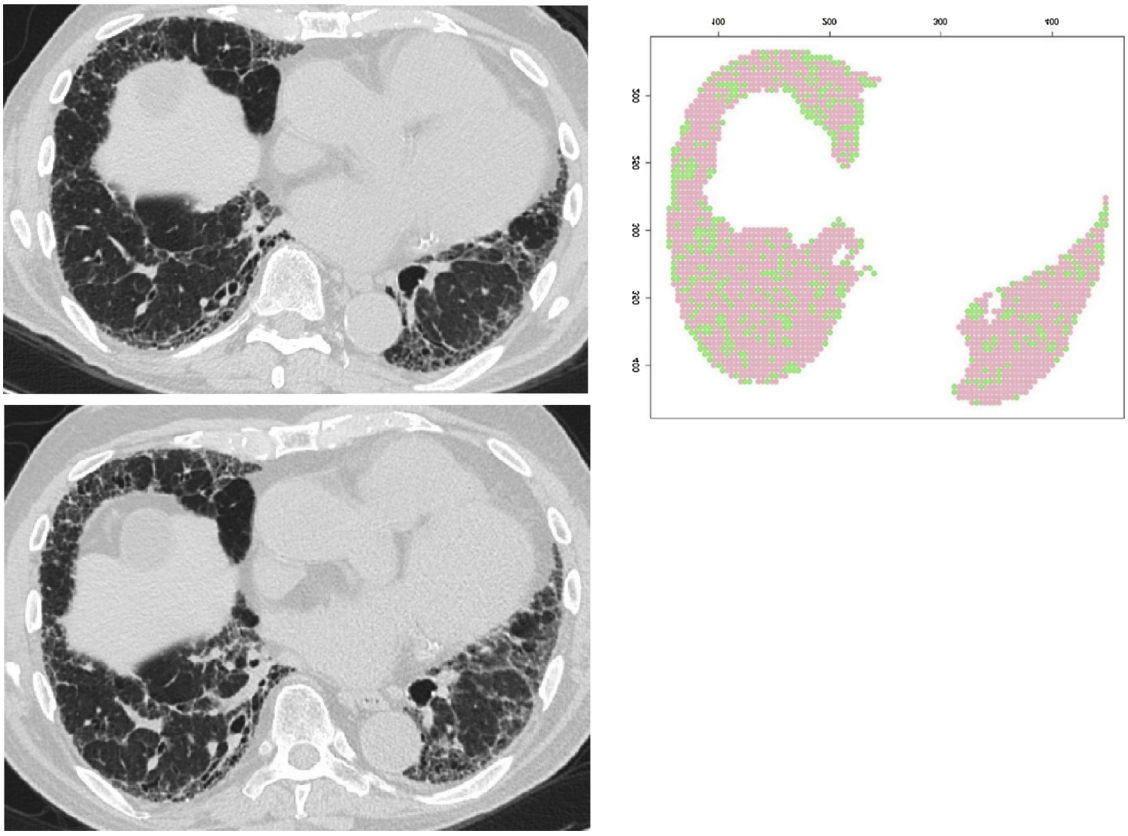

Fig. 5. An expansion to whole lung scan prediction. Top left: baseline CT; bottom left: 9 months follow-up CT; top right: baseline scan with the overlaid result from QPSO-RF model prediction of the expected changes at 9 months (dots with (green) light intensity = voxels classified as expected non-progression, dots with (red) dark intensity = voxels classified as expected progression). In this example, the progression voxels dominate with 75.4% voxels classified as progression.

authors also wish to thank Joshua Lai for the data query and lung segmentation, Dr. Lila Pourzand for the image registration, and Susanne Ventura for proof reading.

Appendix A. Supplementary data

Supplementary material related to this article can be found, in the online version, at doi:https://doi.org/10.1016/j.artmed.2019.101709.

References

[1] Raghu G, Chen SY, Yeh WS, Maroni B, Li Q, Lee YC, et al. Idiopathic pulmonary fibrosis in us medicare beneficiaries aged 65 years and older: incidence, prevalence, and survival, 2001–11. Lancet Respir Med 2014;2(7):566–72.
[2] Raghu G, Collard HR, Egan JJ, Martinez FJ, Behr J, Brown KK, et al. An official ATS/ERS/JRS/ALAT statement: idiopathic pulmonary fibrosis: evidence-based guidelines for diagnosis and management. Am J Respir Crit Care Med 2011;183(6):788–824.
[3] Raghu G, Scholand MB, de Andrade J, Lancaster L, Mageto Y, Goldin J, et al. FG-3019 anti-connective tissue growth factor monoclonal antibody: results of an open-label clinical trial in idiopathic pulmonary fibrosis. Eur Respir J 2016;47(5):1481–91.
[4] Flaherty KR, Colby TV, Travis WD, Toews GB, Mumford J, Murray S, et al. Fibroblastic foci in usual interstitial pneumonia: idiopathic versus collagen vascular disease. Am J Respir Crit Care Med 2003;167(10):1410–5.
[5] Uppaluri R, Homan EA, Sonka M, Hartley PG, Hunninghake GW, McLennan G. Computer recognition of regional lung disease patterns. Am J Respir Crit Care Med 1999;160(2):648–54.
[6] Kim KG, Goo JM, Kim JH, Lee HJ, Min BG, Bae KT, et al. Computer-aided diagnosis of localized ground-glass opacity in the lung at ct: initial experience. Radiology 2005;237(2):657–61.
[7] Kim HJ, Li G, Gjertson D, Elasho R, Shah SK, Ochs R, et al. Classification of parenchymal abnormality in scleroderma lung using a novel approach to denoise images collected via a multicenter study. Acad Radiol 2008;15(8):1004–16.
[8] Kim HJ, Brown MS, Chong D, Gjertson DW, Lu P, Kim HJ, et al. Comparison of the quantitative ct imaging biomarkers of idiopathic pulmonary fibrosis at baseline and early change with an interval of 7 months. Acad Radiol 2015;22(1):70–80.
[9] Tibshirani R. Regression shrinkage and selection via the lasso. J R Stat Soc Ser B 1996:267–88.
[10] Fan J, Li R. Variable selection via nonconcave penalized likelihood and its oracle properties. J Am Stat Assoc 2001;96(456):1348–60.
[11] Mwangi B, Tian TS, Soares JC. A review of feature reduction techniques in neuroimaging. Neuroinformatics 2014;12(2):229–44.
[12] Mehranian A, Rad HS, Rahmim A, Ay MR, Zaidi H. Smoothly clipped absolute deviation (SCAD) regularization for compressed sensing MRI using an augmented lagrangian scheme. Magn Reson Imaging 2013;31(8):1399–411.
[13] Belghith A, Bowd C, Medeiros FA, Balasubramanian M, Weinreb RN, Zangwill LM. Learning from healthy and stable eyes: a new approach for detection of glaucomatous progression. Artif Intell Med 2015;64(2):105–15.
[14] Criminisi A, Shotton J. Decision forests for computer vision and medical image analysis. Springer Science & Business Media 2013.
[15] Furey TS, Cristianini N, Duy N, Bednarski DW, Schummer M, Haussler D. Support vector machine classification and validation of cancer tissue samples using microarray expression data. Bioinformatics 2000;16(10):906–14.
[16] Maglogiannis I, Zaropoulos E, Anagnostopoulos I. An intelligent system for automated breast cancer diagnosis and prognosis using svm based classifiers. Appl Intell 2009;30(1):24–36.
[17] Motai Y. Kernel association for classification and prediction: a survey. IEEE Trans Neural Netw Learn Syst 2015;26(2):208–23.
[18] Utho J, Sieren JC. Information theory optimization based feature selection in breast mammography lesion classification, in: biomedical imaging (ISBI 2018). 2018 IEEE 15th International Symposium on, IEEE 2018:817–21.
[19] Xue B, Zhang M, Browne WN, Yao X. A survey on evolutionary computation approaches to feature selection. Ieee Trans Evol Comput 2016;20(4):606–26.
[20] Sun J, Feng B, Xu W. Particle swarm optimization with particles having quantum behavior. Evolutionary computation, 2004. CEC2004 Vol. 1. IEEE; 2004. p. 325–31. Congress on.
[21] Sun J, Lai CH, Wu XJ. Particle swarm optimisation: classical and quantum perspectives. CRC Press; 2011.
[22] Li Y, Jiao L, Shang R, Stolkin R. Dynamic-context cooperative quantum-behaved particle swarm optimization based on multilevel thresholding applied to medical image segmentation. Inf Sci (Ny) 2015;294:408–22.
[23] Fu Y, Ding M, Zhou C. Phase angle-encoded and quantum-behaved particle swarm optimization applied to three-dimensional route planning for uav, IEEE transactions on systems, man and cybernetics. IEEE Trans Syst Man Cybern A Syst Hum 2012;42(2):511–26.
[24] Lukemire J, Mandal A, Wong WK. d-qpso: a quantum-behaved particle swarm technique for finding D-optimal designs with discrete and continuous factors and a

binary response. Technometrics 2018:1–27.
[25] Xi M, Sun J, Xu W. An improved quantum-behaved particle swarm optimization algorithm with weighted mean best position. Appl Math Comput 2008;205(2):751–9.
[26] Jin C, Jin S-W. Prediction approach of software fault-proneness based on hybrid artificial neural network and quantum particle swarm optimization. Appl Soft Comput 2015;35:717–25.
[27] Guo Y, Liu Y, Oerlemans A, Lao S, Wu S, Lew MS. Deep learning for visual understanding: a review. Neurocomputing 2016;187:27–48.
[28] McNitt-Gray MF, Huang H, Sayre JW. Feature selection in the pattern classification problem of digital chest radiograph segmentation. IEEE Trans Med Imaging 1995;14(3):537–47.
[29] Yuan M, Lin Y. Model selection and estimation in regression with grouped variables. J R Stat Soc Series B Stat Methodol 2006;68(1):49–67.
[30] Peng H, Long F, Ding C. Feature selection based on mutual information criteria of max-dependency, max-relevance, and min-redundancy. IEEE Trans Pattern Anal Mach Intell 2005;27(8):1226–38.
[31] Saeys Y, Inza I, Larra～naga P. A review of feature selection techniques in bioinformatics. bioinformatics 2007;23(19):2507–17.
[32] Cho BH, Yu H, Kim K-W, Kim TH, Kim IY, Kim SI. Application of irregular and unbalanced data to predict diabetic nephropathy using visualization and feature selection methods. Artif Intell Med 2008;42(1):37–53.
[33] Mi H, Petitjean C, Dubray B, Vera P, Ruan S. Robust feature selection to predict tumor treatment outcome. Artif Intell Med 2015;64(3):195–204.
[34] John GH, Kohavi R, Pfleger K, et al. Irrelevant features and the subset selection problem. Machine Learning: Proceedings of the Eleventh International Conference 1994:121–9.
[35] Liu H, Yu L. Toward integrating feature selection algorithms for classification and clustering. IEEE Trans Knowl Data Eng 2005;17(4):491–502.
[36] Kohavi R, John GH. Wrappers for feature subset selection. Artif Intell 1997;97(1–2):273–324.
[37] Kennedy J, Eberhart RC. A discrete binary version of the particle swarm algorithm. Systems, Man, and Cybernetics, 1997. Computational Cybernetics and Simulation., 1997 IEEE International Conference on, Vol. 5. 1997. p. 4104–8.
[38] Nguyen HB, Xue B, Andreae P, Zhang M. Particle swarm optimisation with genetic operators for feature selection. Evolutionary computation (CEC), 2017 IEEE Congress on, IEEE. 2017. p. 286–93.
[39] Mura M, Porretta MA, Bargagli E, Sergiacomi G, Zompatori M, Sverzellati N, et al. Predicting survival in newly diagnosed idiopathic pulmonary fibrosis: a 3-year prospective study. Eur Respir J 2012:erj01060–2011.
[40] Robbie H, Daccord C, Chua F, Devaraj A. Evaluating disease severity in idiopathic pulmonary fibrosis. Eur Respir Rev 2017;26(145):170051.
[41] King Jr TE, Bradford WZ, Castro-Bernardini S, Fagan EA, Glaspole I, Glassberg MK, et al. A phase 3 trial of pirfenidone in patients with idiopathic pulmonary fibrosis. N Engl J Med 2014;370(22):2083–92.
[42] Haralick RM. Statistical and structural approaches to texture. Proceedings of the IEEE 1979:786–804. 67 (5).
[43] Chabat F, Yang G-Z, Hansell DM. Obstructive lung diseases: texture classification for differentiation at CT. Radiology 2003;228(3):871–7.
[44] Sonka M, Hlavac V, Boyle R. Image processing, analysis, and machine vision. Cengage Learning; 2014.
[45] Liang P. Semi-supervised learning for natural language PhD. thesis Massachusetts Institute of Technology; 2005.
[46] Silva I, Moody G, Scott DJ, Celi LA, Mark RG. Predicting in-hospital mortality of ICU patients: the physionet/computing in cardiology challenge 2012. Comput Cardiol (2010) 2012;39:245.
[47] Sun J, Xu W, Fang W, Chai Z. Quantum-behaved particle swarm optimization with binary encoding. Adaptive and Natural Computing Algorithms 2007:376–85.
[48] Zhao J, Sun J, Xu W. A binary quantum-behaved particle swarm optimization algorithm with cooperative approach. International Journal of Computer Science 2013;10(1):112–8.
[49] Suganthan PN. Particle swarm optimiser with neighbourhood operator. Evolutionary computation, 1999. CEC 99 Vol. 3. IEEE; 1999. p. 1958–62. Proceedings of the 1999 Congress on.
[50] Rohler AB, Chen S. An analysis of sub-swarms in multi-swarm systems. Australasian Joint Conference on Artificial Intelligence 2011:271–80.
[51] Breiman L. Random forests. Mach Learn 2001;45(1):5–32.
[52] Desir C, Bernard S, Petitjean C, Heutte L. A random forest based approach for one class classification in medical imaging. International workshop on machine learning in medical imaging. Springer; 2012. p. 250–7.
[53] Lebedev A, Westman E, Van Westen G, Kramberger M, Lundervold A, Aarsland D, et al. Random forest ensembles for detection and prediction of alzheimer's disease with a good between-cohort robustness. Neuroimage Clin 2014;6:115–25.
[54] Zhang R, Shen J, Wei F, Li X, Sangaiah AK. Medical image classification based on multi-scale non-negative sparse coding. Artif Intell Med 2017;83:44–51.
[55] Hussain MA, Bhuiyan A, Luu CD, Smith RT, Guymer RH, Ishikawa H, et al. Classification of healthy and diseased retina using sd-oct imaging and random forest algorithm. PLoS One 2018;13(6):e0198281.
[56] Dietterich TG. An experimental comparison of three methods for constructing ensembles of decision trees: bagging, boosting, and randomization. Mach Learn 2000;40(2):139–57.
[57] Friedman J, Hastie T, Tibshirani R. The elements of statistical learning Vol. 1. Berlin: Springer series in statistics Springer; 2001.
[58] Chawla NV, Bowyer KW, Hall LO, Kegelmeyer WP. Smote: synthetic minority oversampling technique. J Artif Intell Res 2002;16:321–57.
[59] Hosmer Jr DW, Lemeshow S, Sturdivant RX. Applied logistic regression Vol. 398. John Wiley & Sons; 2013.
[60] Huber PJ, et al. The behavior of maximum likelihood estimates under nonstandard conditions. Proceedings of the Fth Berkeley Symposium on Mathematical Statistics and Probability 1967:221–33. Vol. 1.
[61] Benjamini Y, Hochberg Y. Controlling the false discovery rate: a practical and powerful approach to multiple testing, Journal of the royal statistical society. Series B (Methodological) 1995:289–300.
[62] L. B. Booker, D. E. Goldberg, J. H. Holland, Classier systems and genetic algorithms.
[63] Yang J, Honavar V. Feature subset selection using a genetic algorithm, in: feature extraction, construction and selection. Springer; 1998. p. 117–36.
[64] Hassan R, Cohanim B, De Weck O, Venter G. A comparison of particle swarm optimization and the genetic algorithm. 46th AIAA/ASME/ASCE/AHS/ASC Structures, Structural Dynamics and Materials Conference 2005:1897.
[65] Ley B, Ryerson CJ, Vittingho E, Ryu JH, Tomassetti S, Lee JS, et al. A multidimensional index and staging system for idiopathic pulmonary fibrosis. Ann Intern Med 2012;156(10):684–91.
[66] Tashkin DP, Volkmann ER, Tseng C-H, Kim HJ, Goldin J, Clements P, et al. Relationship between quantitative radiographic assessments of interstitial lung disease and physiological and clinical features of systemic sclerosis. Ann Rheum Dis 2016;75(2):374–81.